Journal of Rock Mechanics and Geotechnical Engineering 14 (2022) 953–966

Contents lists available at ScienceDirect

Journal of Rock Mechanics and Geotechnical Engineering

journal homepage: www.jrmge.cn

Full Length Article

Structural, volumetric and water retention behaviors of a compacted clay upon saline intrusion and freeze-thaw cycles

Jianguo Lin [a], Weilie Zou [a,b,*], Zhong Han [a,b,**], Ziwei Zhang [a], Xiequn Wang [c]

[a] School of Civil Engineering, Wuhan University, Wuhan, 430072, China
[b] Key Laboratory of Hydraulic Rock Mechanics of Ministry of Education, Wuhan University, Wuhan, 430072, China
[c] School of Civil Engineering and Architecture, Wuhan University of Technology, Wuhan, 430070, China

ARTICLE INFO

Article history:
Received 5 May 2021
Received in revised form
4 August 2021
Accepted 2 December 2021
Available online 19 January 2022

Keywords:
Compacted clay
Microstructure
Volumetric behavior
Water-retention capacity
Salinization
Freeze-thaw (FT) cycles

ABSTRACT

This study investigates the evolution of the structural, volumetric and water retention behaviors of a compacted clay during soaking and desiccation considering the influences of freeze-thaw (FT) cycles and saline intrusion. Compacted specimens were subjected to different FT cycles and then submerged in NaCl solution with different concentrations to facilitate the saline intrusion and measure the swelling behaviors. Shrinkage curve and filter paper tests were thereafter performed to reveal the clay's volumetric and water-retention characteristics during desiccation. Mercury intrusion porosimetry and field emission scanning electron microscopy tests were conducted to observe the evolution of the clay's microstructure. Experimental results show that the clay's micropores decrease and macropores increase after FT cycles, which is associated with the migration of water, growth of ice crystals, and development of FT-induced cracks during FT cycles. Similar observations were obtained from specimens after the saline intrusion, which is attributed to the osmotic and osmotically-induced consolidation. FT-induced cracks significantly reduce the clay's swelling and shrinkage potentials. FT cycles result in the shrinkage of micropores which leads to a reduction in the water retention capacity in the low suction range (capillary regime). The salinization suppresses the swelling of the clay and prolongs its primary and secondary swelling stages. The shrinkage potential initially increases and then decreases with increasing saline concentration. Salinization has significant influences on the osmotic suction and thus alters the clay's water-retention curves in terms of total suction. It demonstrates little impact on the clay's water-retention curves in terms of matric suction.

1. Introduction

Compacted clays are widely used in barrier and liner systems for landfills and disposal repositories in geoenvironmental engineering due to their low permeability and self-healing properties against cracking (Daniel and Wu, 1993; Deneele et al., 2010; Jobmann et al., 2017; Julina and Thyagaraj, 2020). The intrusion of salinity from the environment (e.g. leachate from waste, fertilization, etc.) poses severe influences on the hydro-mechanical properties of compacted clays (Bolt, 1955; Basma et al., 1996; Castellanos et al., 2008; Rao and Thyagaraj, 2010; Cui and Tang, 2013; Thyagaraj and Rao, 2013; Mishra et al., 2019).

The as-compacted structure of clays in barriers and liners is typically homogenous and dispersed (Mitchell et al., 1965; Monroy et al., 2010; Romero et al., 2011). Upon saline intrusion, the as-compacted structure may transfer into an aggregated and densely stacked structure with clay particles becoming flocculated (Palomino and Santamarina, 2005; Lyu et al., 2020). Such alternation is more significant when the saline concentration is high (Musso et al., 2013; Mokni et al., 2014). Some researchers attribute this behavior to the suppression of adsorption water film upon the increase in the ion concentration based on the electric double layer theory (Palomino and Santamarina, 2005; Rao et al., 2006; Mokni et al., 2014; Thyagaraj et al., 2017). Such structural changes lead to a reduction in the swelling potential but an increase in the

* Corresponding author. School of Civil Engineering, Wuhan University, Wuhan, 430072, China.
** Corresponding author. School of Civil Engineering, Wuhan University, Wuhan, 430072, China.
E-mail addresses: zwilliam@whu.edu.cn (W. Zou), zhong.han@whu.edu.cn (Z. Han).

Peer review under responsibility of Institute of Rock and Soil Mechanics, Chinese Academy of Sciences.

https://doi.org/10.1016/j.jrmge.2021.12.012

permeability of the intruded clay (Di Maio, 1996; Musso et al., 2003; Rao and Thyagaraj, 2007; He et al., 2016; Zou et al., 2018a).

Barbour and Fredlund (1989) proposed two mechanisms to illustrate the effects of saline intrusion on soils' volumetric behaviors: osmotic consolidation due to changes in the electrostatic stresses between clay particles, and osmotically-induced consolidation that is associated with the drainage of the pore fluid triggered by the osmotic pressure gradient. Some researchers regarded the osmotic pressure gradient as an equivalent stress variable to interpret the strain and settlement induced by the intrusion of salinity solution (Rao and Thyagaraj, 2007; Thyagaraj et al., 2017).

Existing researches on clays' shrinkage behaviors upon dessication mainly focus on factors such as mineral composition, clay particle content, initial soil structure, and hydraulic and stress histories (Boivin et al., 2004; Cornelis et al., 2006; Chertkov, 2007; Alaoui et al., 2011; Leong and Wijaya, 2015). Studies on the shrinkage behaviors of clays intruded by saline solutions are comparatively less reported in the literature.

For the shrinkage behavior, which is mainly indicated by the shrinkage curve (i.e. relationships between soils' volume and moisture content during desiccation), experimental observations on salinized soils vary. For example, Zhang et al. (2017) obtained similar shrinkage curves from slurried silty clay specimens prepared with NaCl solutions of different concentrations and suggested that NaCl solutions have little impact on shrinkage curves. On the contrary, Thyagaraj et al. (2017) reported that the magnitude of osmotic suction and the type of pore fluid impose critical influences on the shrinkage behavior of compacted expansive clays. Besides, Julina and Thyagaraj (2020) evaluated the combined effects of pore fluid and cyclic wetting-drying (WD) cycles on the desiccation cracks of a compacted clay. They found that after WD cycles, clay specimens inundated with 4 mol/L NaCl solution developed more desiccation cracks than those inundated with distilled water or 0.4 mol/L NaCl solution.

The soil-water retention curve (SWRC) defines the relationships between soils' moisture content and suction and is the key property indicating soils' water retention capacity. Capillary effects (mainly associated with soils' pore structure) dominate the SWRC in the low suction range, while adsorption effects (mainly associated with soils' mineralogical composition, cation exchange capacity, and surficial properties) control the SWRC in the high suction range (Romero et al., 1999, 2011; Birle et al., 2008; Lu and Khorshidi, 2015; Lu, 2016; Han and Vanapalli, 2017; Lu and Dong, 2017; Zou et al., 2018b; Molinero-Guerra et al., 2020). Thyagaraj and Sudhakar (2010) reported that the swelling potential and water retention capacity of an expansive clay decrease upon the infiltration of salt solutions. He et al. (2016) reported for a clay that at a given suction in the high suction range, the degree of saturation of specimens increases with the increase in salt concentration. Mokni et al. (2014) obtained similar SWRC in the high suction range for the compacted illitic-kaolinitic clay samples prepared with $NaNO_3$ solutions of different concentrations. Zhang et al. (2017) found that the matric suction in the low range was not sensitive to the pore fluid.

In cold regions, the effects of cyclic freeze-thaw (FT) actions on the hydro-mechanical properties of compacted clays are of great concern. It is widely recognized that during FT cycles, the void ratio increases for dense soils while decreases for loose soils, the permeability always increases irrespective of the volumetric changes, and the shear strength declines remarkably (Chamberlain and Gow, 1979; Konrad, 1989; Qi et al., 2006; Gens, 2010; Liu et al., 2016; Ren et al., 2017; Dalla et al., 2019). Besides, FT actions change the microstructure of soils by introducing FT-induced macropores and fissures and leads to a reduction in soils' water retention capacity and the scale of swelling and shrinkage upon moisture fluctuation (Ding et al., 2020; Zou et al., 2020b). Saline intrusion and FT actions pose significant yet different influences on the structural, volumetric and water retention behaviors of compacted clays. However, few studies have focused on their joint effects despite their significance in the design of earthen barrier and liner systems in cold regions.

Table 1
Physical properties of the tested clay.

Property	Value
Specific gravity, G_s	2.68
Liquid limit, w_L (%)	45
Plastic limit, w_P (%)	23
Plasticity index, I_P (%)	22
Maximum dry density, ρ_{dmax} (g/cm^3)	1.6
Optimum water content, w_{opt} (%)	22.76
Sand content (%)	10
Silt content (%)	54
Clay content (%)	26
Unified soil classification system (USCS) classification	CL

This study aims at investigating the influences of FT cycles on the microstructure, swelling and shrinkage behaviors, and water retention capacity of a compacted clay that is intruded by NaCl solutions of different concentrations. Compacted clay specimens were first subjected to different FT cycles and then submerged in pure water or NaCl solutions to record the swelling behavior. Saturated specimens were thereafter air-dried under room temperature during which the variations in the volume and suction with decreasing moisture content were measured to establish the shrinkage curve and SWRC, respectively. Mercury intrusion porosimetry (MIP) and field emission scanning electron microscopy (FESEM) tests were conducted to observe the evolution in the clay's microstructure during FT cycles, saline intrusion and the subsequent drying processes to explain the responses of the clay from microscopic perspectives.

2. Materials and methods

2.1. Materials and specimen preparation

The clay investigated in this study was collected from Heilongjiang Province in northeastern China. Clay samples were air-dried, pulverized, and then passed through a 2 mm sieve to

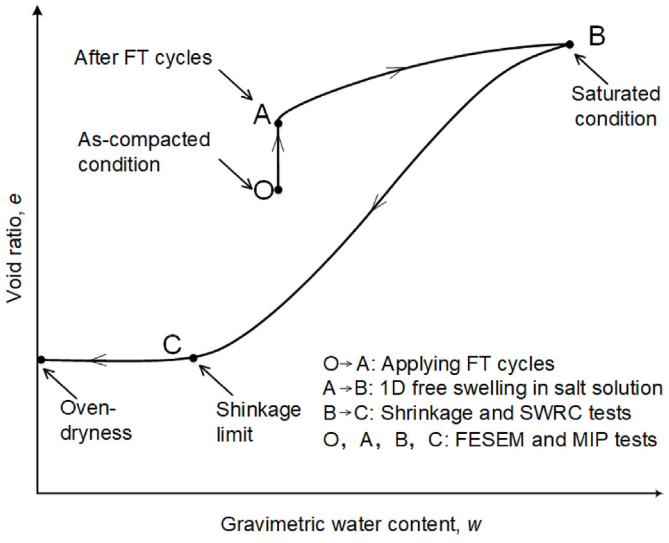

Fig. 1. Testing sequence in this study. 1D represents 'one-dimensional'.

remove larger particles and debris. The processed clay was subjected to a series of laboratory experiments to determine the basic physical properties (Table 1). X-ray analysis shows that the clay mineral content (% by mass) is 12% for the montmorillonite, 3% for the illite, 2% for the kaolinite, and 1% for the chlorite.

The dry clay powder was thoroughly mixed with distilled water to attain the clay's optimum water content (w_{opt} = 22.76%). The moist soil was statically compacted to the maximum dry density (ρ_{dmax} = 1577 kg/m^3) in oedometer rings of 61.8 mm in diameter and 20 mm in height. The initial void ratio of the specimens was 0.66. Compacted specimens were immediately wrapped in layers of plastic membrane to prevent evaporation.

Fig. 1 shows the testing sequence in this study. As-compacted specimens were first subjected to different numbers of FT cycles ($O \rightarrow A$). FT-impacted specimens were submerged in pure water or NaCl solutions with different concentrations to facilitate the saline intrusion and the measurement of the swelling behaviors ($A \rightarrow B$). Saturated specimens were air-dried to the shrinkage limit ($B \rightarrow C$) and then further dried in an oven to achieve oven-dryness. The shrinkage curves and SWRCs were measured during the desiccation. MIP and FESEM tests were performed at points O, A, B and C in Fig. 1 to trace the structural evolution of the clay.

2.2. Application of FT cycles

FT cycles were applied in an environmental chamber with precise temperature control. In one FT cycle, specimens were frozen at −20 °C for 12 h and thawed at 20 °C for 12 h. The chosen temperature range was determined referencing the local average temperature records in Heilongjiang, which was between 23.1 °C in summer and −18.6 °C in winter. The 12 h is considered adequate for achieving equilibrium of temperature and moisture in small size specimens such as the disc specimens used in this study (Lu et al., 2019; Ding et al., 2020; Zou et al., 2020b).

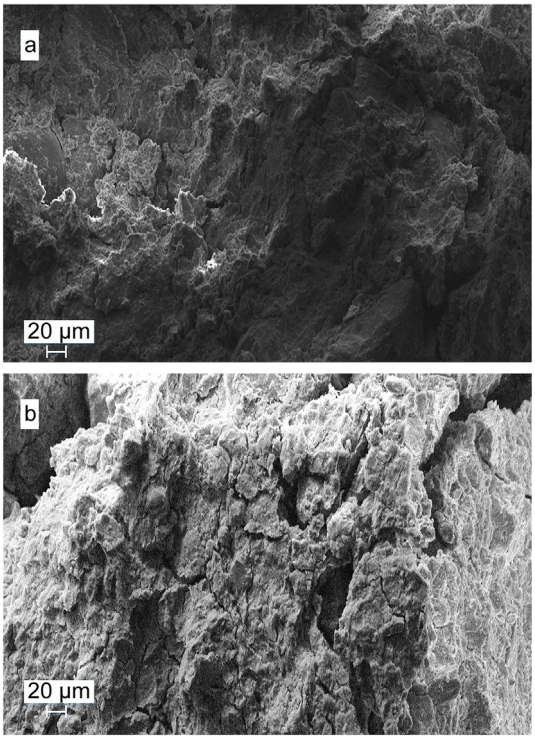

Fig. 2. FESEM images of (a) as-compacted specimen and (b) specimen after 10 FT cycles.

All FT cycles were applied at free stress state. In other words, no external stress was applied. This is because the in situ soils subjected to FT actions are mainly in the shallow depth where the stress level is low. Such external stress level is much smaller than the internal stress caused by the growth of ice crystals during freezing and thus imposes a much lower impact on soils' mechanical behaviors compared to FT cycles. In addition, during freezing, the development of cracks and swelling is most significant when there is no external stress. Thus, the nil stress state represents the worst-case scenario for the degradation in soils' mechanical properties.

Compacted clays used in liner and barrier systems typically are very low in permeability. Upon FT processes, the migration of water in the clay layer is limited, especially during rapid temperature drop. In other words, the moisture content remains approximately constant during FT cycles. Therefore, closed-system FT cycles (i.e. no moisture exchange with the surrounding environment) are commonly used to impose FT histories to clays (Chamberlain, 1973). During closed-system FT cycles, soils' structure and hydromechanical properties experience dramatic changes during the first FT cycle. The changes level off after about 5–7 cycles (Chamberlain

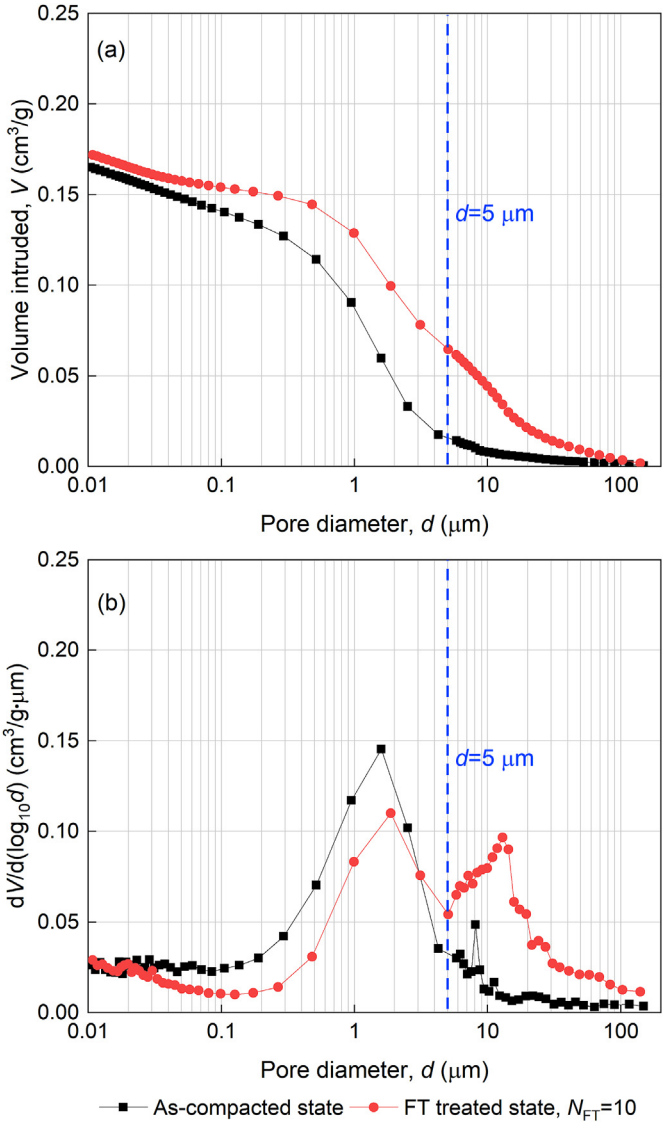

Fig. 3. MIP results before and after FT action: (a) CI curves, and (b) PSD curves.

Table 2
Intruded volume at different states.

N_{FT}	State	Intruded volume of micropores, V_m (cm^3/g)		Intruded volume of macropores, V_M (cm^3/g)	
		c = 0 mol/L	c = 3 mol/L	c = 0 mol/L	c = 3 mol/L
0	As-compacted	0.1551	0.1551	0.0143	0.0143
	Saturated	0.2014	0.1351	0.038	0.0424
	Air-dried	0.0842	0.0766	0.0166	0.0206
10	FT treated	0.1131	0.1131	0.0647	0.0647
	Saturated	0.1242	0.0606	0.0483	0.0743
	Air-dried	0.0672	0.0584	0.0609	0.073

and Gow, 1979; Qi et al., 2006). In this study, three designated FT cycles (i.e. N_{FT} = 0, 1 and 10) were applied to reveal the changes in clay's behaviors from as-compacted condition (N_{FT} = 0) to the equilibrium condition after FT cycles (N_{FT} = 10), highlighting the most significant changes at N_{FT} = 1. During FT processes, specimens were confined in oedometer rings and sealed in plastic membranes to facilitate the closed-system FT processes.

2.3. Saline intrusion and swelling test

After FT cycles, specimens were confined in oedometer rings and submerged in distilled water (concentration c = 0 mol/L) or NaCl solution with different c values (c = 0.1 mol/L, 0.5 mol/L and 3 mol/L) in an oedometer to facilitate the saline intrusion and determine the 1D swelling behavior under a token load of 1 kPa. A dial gauge and a timer were used to monitor the development of vertical deformation (i.e. the volume of specimens) with time. Specimens were soaked for at least 5 d and until the change in the dial gauge readings was less than 0.01 mm over 24 h (i.e. strain rate <0.05% per day) following ASTM D4546-14 (2019). The degree of saturation of specimens after such soaking procedure was 95%–100%, confirming that the saturated condition has been achieved within the tested specimens.

2.4. Measurement of the shrinkage curve

Saturated specimens were retrieved from oedometer rings and placed on perforated plastic plates at room temperature to dry in the air at room temperature of 20 °C. Their mass and dimension were periodically measured using a balance readable to 0.01 g and a digital vernier caliper readable to 0.005 mm, respectively. Such an approach measures the global volume of soils (including the volume of soil solids, voids and cracks) and is different from approaches such as the balloon method (Toker et al., 2004; Cornelis et al., 2006) which measure the volume of structureless soils or soil matrix.

It generally took 5 d for the specimens to dry from fully saturated condition to the shrinkage limit. The shrinkage limit was deemed achieved when specimens stopped shrinking and their mass stopped decreasing, per the criterion outlined in the Chinese Standards for Geotechnical Testing Method GB/T 50123-2019 (2019). Specimens were thereafter transferred to an oven to dry at 105 °C for 24 h to achieve oven-dryness. Mass and dimension measurements during drying were used to determine the moisture content and volumetric strain of the clay during desiccation and thus establish the shrinkage curve.

2.5. Measurement of the SWRCs

Contact and non-contact filter paper methods using Whatman 42 filter papers were employed to measure the variation in the matric suction (s_m) and total suction (s) with moisture content per

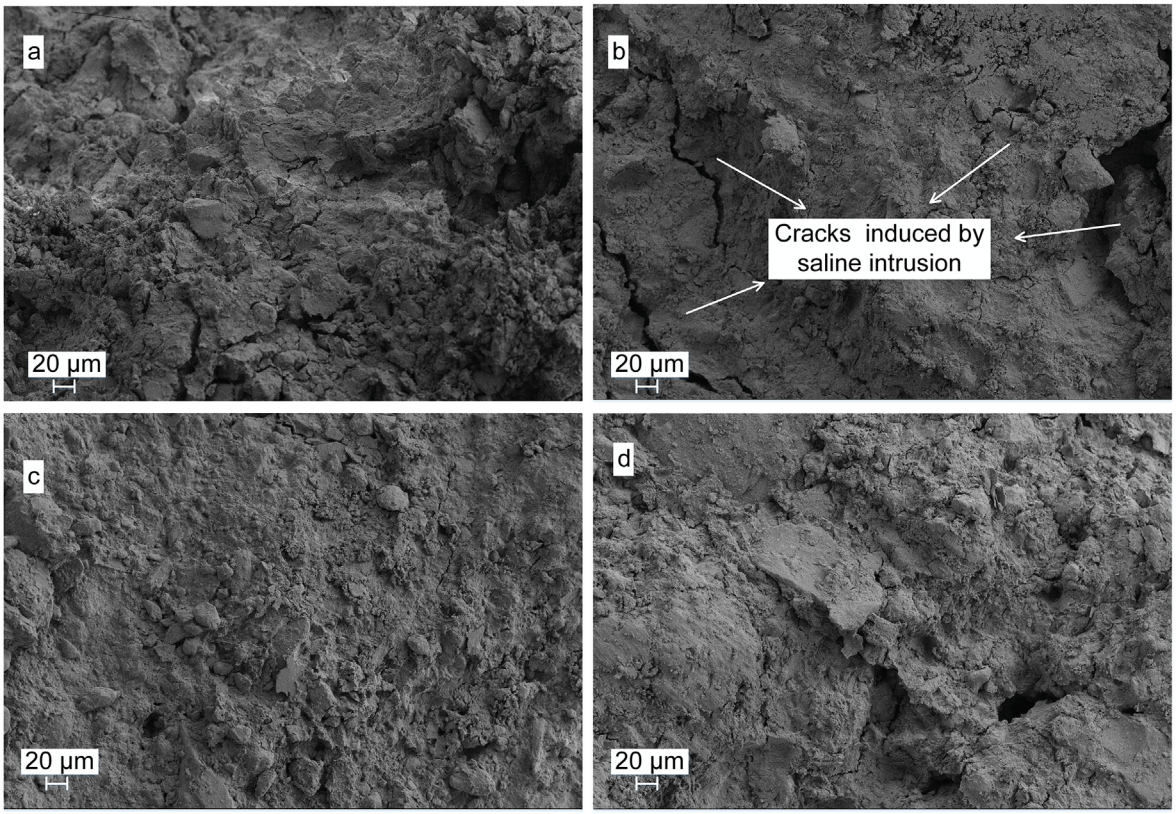

Fig. 4. FESEM images: (a) Saturated state, N_{FT} = 0, c = 0 mol/L; (b) Saturated state, N_{FT} = 0, c = 3 mol/L; (c) Air-dried state, N_{FT} = 0, c = 0 mol/L; and (d) Air-dried state, N_{FT} = 0, c = 3 mol/L.

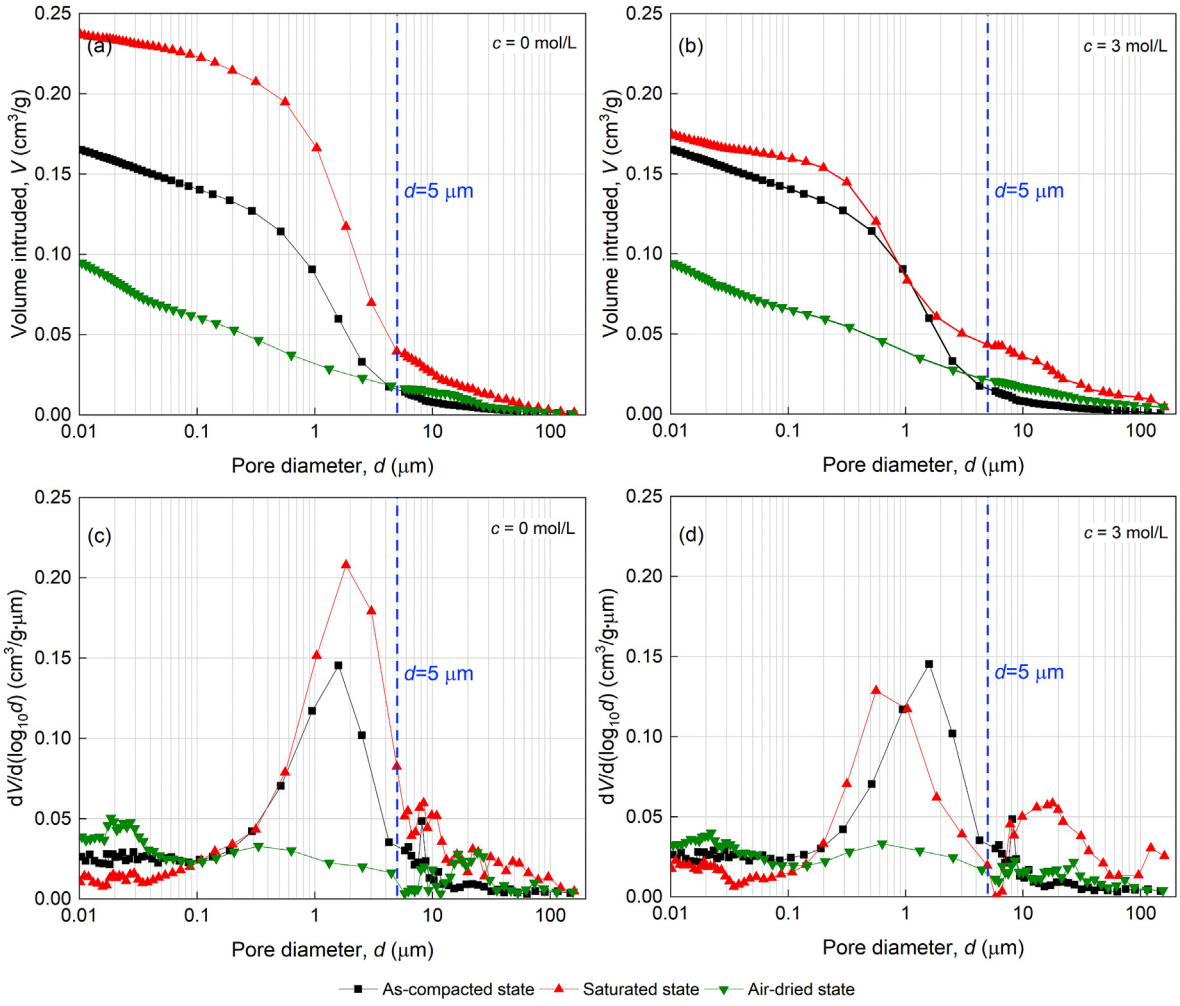

Fig. 5. MIP results of specimens without FT cycles: (a) CI curves at $c = 0$ mol/L, (b) CI curves at $c = 3$ mol/L, (c) PSD curves at $c = 0$ mol/L, and (d) PSD curves at $c = 3$ mol/L.

ASTM D5298-10 (2010), respectively. Considering that measuring suction using the filter paper method is time-consuming, only three levels of salt concentrations (i.e. 0 mol/L, 0.1 mol/L and 3 mol/L) were imposed on tested specimens. Specimens and filter papers were sealed in plastic containers for at least 10 d to achieve moisture equilibrium. The measured s_m and s can be used to determine the clay's osmotic suction s_o ($= s - s_m$). The s_o can also be obtained from Van't Hoff's theory as follows:

$$s_o = icRT \tag{1}$$

where i is the Van't Hoff factor, and $i = 2$ for NaCl solutions (Rao and Shivananda, 2005); R is the universal gas constant and equals 8.314 J/(mol K); and T is the absolute temperature.

2.6. Microstructural observation

MIP and FESEM tests were carried out on specimens at as-compacted state ($N_{FT} = 0$) and equilibrium state after FT cycles ($N_{FT} = 10$), and specimens inundated with distilled water ($c = 0$ mol/L) or NaCl solution ($c = 3$ mol/L) at the saturated state and air-dried state. MIP tests determine the clay's cumulative intruded volume (CI) curve (i.e. intruded volume per unit mass of soil, V versus pore size, d, relationships) and the pore size distribution (PSD) curve (i.e. the derivatives of the CI curves, $dV/d(\log_{10}d)$ versus d relationships). Small soil blocks were sampled from the disc specimens and were freeze-dried in liquid nitrogen to preserve the structure before submitting to MIP and FESEM tests.

3. Results and discussions

3.1. Clay's microstructural behaviors

3.1.1. Evolution of the microstructure during FT cycles

Fig. 2 shows the FESEM images of the as-compacted specimens and specimens after 10 FT cycles. The as-compacted clay presents a homogenous structure (Fig. 2a), while after 10 FT cycles, the structure becomes segragated with visible cracks. The cracks present dimensions of approximately 20 μm. The presence of the cracks is associated with the development of ice crystals during freezing, which segregates the soil structure and causes irreversible large space and cracks (Chamberlain and Gow, 1979; Qi et al., 2006). Such change is also reflected in the clay's global volume. The void ratio (e) increased from 0.66 for the as-compacted specimen to 0.68 after 1 FT cycle and to 0.71 after 10 FT cycles.

Fig. 3 summarizes the MIP results. The PSD curve of the as-compacted specimens is generally unimodal with a peak close to 2 μm. It evolves into a bimodal fashion after 10 FT cycles which features an existing peak at 2 μm and a new peak between 10 μm and 20 μm. It is noted that 10–20 μm is the dimension of the FT-induced cracks shown in Fig. 2. Thus, this new peak indicates FT-

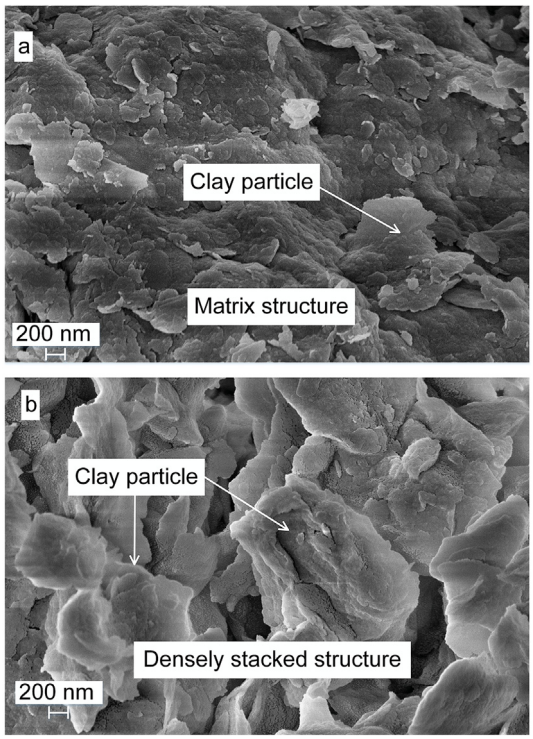

Fig. 6. FESEM images at saturated state: (a) $N_{FT} = 0$, $c = 0$ mol/L; and (b) $N_{FT} = 0$, $c = 3$ mol/L.

induced cracks. The two peaks are divided at $d = 5$ μm, which is also the turning point of the CI curves of the specimens before and after FT cycles. Burton et al. (2015) suggested using the turning point of the CI and PSD curves as the boundary between clays' macropores and micropores. It is shown in following sections that the CI and PSD curves of the clay after saturation and desiccation also turn at 5 μm. Due to this reason, 5 μm is defined as the delimiting boundary separating the macropores and micropores.

The intruded volume of macropores (V_M) and micropores (V_m) can be identified from the CI curves shown in Fig. 3a and are summarized in Table 2. Micropores slightly shrink after FT cycles, which is demonstrated by a reduction in the V_m from 0.1551 at $N_{FT} = 0$ to 0.1131 at $N_{FT} = 10$ (i.e. decreased by 27%) and the downshifting of the PSD curves (Fig. 3b). On the contrary, due to the development of FT-induced cracks, the volume of macropores significantly increases after FT cycles. The V_M rises from 0.0143 at $N_{FT} = 0$ to 0.0647 at $N_{FT} = 10$ (i.e. increased by 352%). It can be seen that FT cycles impose more significant influences on the macropore system than the micropore system.

During freezing, pore water stored in macropores freezes first while the pore water in micropores remains unfrozen (Konrad, 1989; Liu et al., 2016). Due to this reason, the water potential within macropores is lower than that within micropores, which results in the migration of unfrozen water from micropores towards the macropores and facilitates the growth of ice crystals. The development of ice crystals enlarges the macropores consequently. Due to the loss of unfrozen water, the suction within micropores continues to increase, leading to the shrinkage of the micropores (Zou et al., 2020b).

3.1.2. *Influences of salinization on the microstructure of specimens without FT histories*

This section discusses the evolution of the microstructure of as-compacted specimens (i.e. without FT histories) during the saturation and desiccation processes. Fig. 4 shows the FESEM images of the as-compacted clay at the saturated condition and the shrinkage limit. The corresponding CI and PSD curves are summarized in Fig. 5 and the V_M and V_m are summarized in Table 2.

The soil structure does not change significantly upon soaking in distilled water (Figs. 2a and 4a). There is a slight increase in the volume of micropores due to the thickening of the electric double layer between soil particles (Delage et al., 2006) and macropore owing to the swelling of the soil skeleton. Correspondingly, V_M and V_m values increase and the PSD curve generally shifts upward (Table 2 and Fig. 5c).

On the contrary, as-compacted specimens soaked in NaCl solution ($c = 3.0$ mol/L) develop visible large pore spaces (Fig. 4b). It is important to note that the NaCl dissolved in the clay's pore fluid precipitates upon freeze-drying. The solid NaCl crystals reduces V_M and V_m. The V_M increases (Table 2) and the PSD curve develops a new peak between 10 μm and 20 μm (Fig. 5d). Meanwhile, the soil matrix becomes denser compared to specimens soaked in distilled water (Fig. 4a and b), which is corroborated by the slight decrease in V_m. In general, the global volume of the specimens swells slightly (i.e. $V_M + V_m$ increases) after saturation.

The shrinkage of micropores and the increase in macropores are associated with saline intrusion. As shown in Fig. 6a, clay particles and their structure become uniform when saturated in distilled water. However, in the 3 mol/L NaCl solution, the saline suppresses the water adsorption to the surface of clay particles and thus reduces the thickness of the electric double layer. The clay particles become densely stacked and flocculated, leaving visible space among them (Fig. 6b) that transfers to macropores (Palomino and Santamarina, 2005). This phenomenon fits the description of osmotic consolidation (Barbour and Fredlund, 1989).

At air-dried state, macropores and micropores shrink significantly for specimens saturated in water and 3 mol/L NaCl solution, as can be judged from FESEM images in Figs. 4c and 4d, the decreases in V_M and V_m in Table 2, and the flattening of the PSD curves in Figs. 5c and 5d. It is noted that the increase in macropores due to saline intrusion is reversible upon desiccation, and the shrinkage of micropores lead to an increase in the number of pores smaller than 0.05 μm (PSD curves in Fig. 5).

3.1.3. *Influences of salinization on the microstructure of specimens with FT histories*

This section discusses the evolution of the microstructure during saturation and desiccation for specimens that have been subjected to 10 FT cycles (i.e. with FT histories). Fig. 7 shows the FESEM images of the specimens at the saturated condition and the shrinkage limit. The corresponding CI and PSD curves are summarized in Fig. 8 and the V_M and V_m obtained from CI curves are summarized in Table 2.

The V_m of FT-impacted specimens increases after soaking in distilled water, indicating the swelling of micropores. Meanwhile, the V_m decreases after soaking in 3 mol/L NaCl solution, indicating the shrinkage of micropores. Such behaviors are similar to that of specimens without FT histories. For macropores, the behaviors upon soaking are different. The V_M decreases in distilled water, meaning a reduction in the macropore spaces. This is possibly associated with two reasons: (i) FT actions reduce the integrity of the soil skeleton and thus reduce the swelling or even induce the partial collapse of the soil skeleton upon soaking, and (ii) the soil matrix swells and occupies the space of macropore and FT-induced cracks. Comparing Figs. 2b and 7a, it can be observed that the cracks are narrowed after soaking.

On the other hand, the V_M slightly increases in the 3 mol/L NaCl solution, meaning that the volume of macropore remains stable upon saturation. This is related to the osmotic consolidation upon

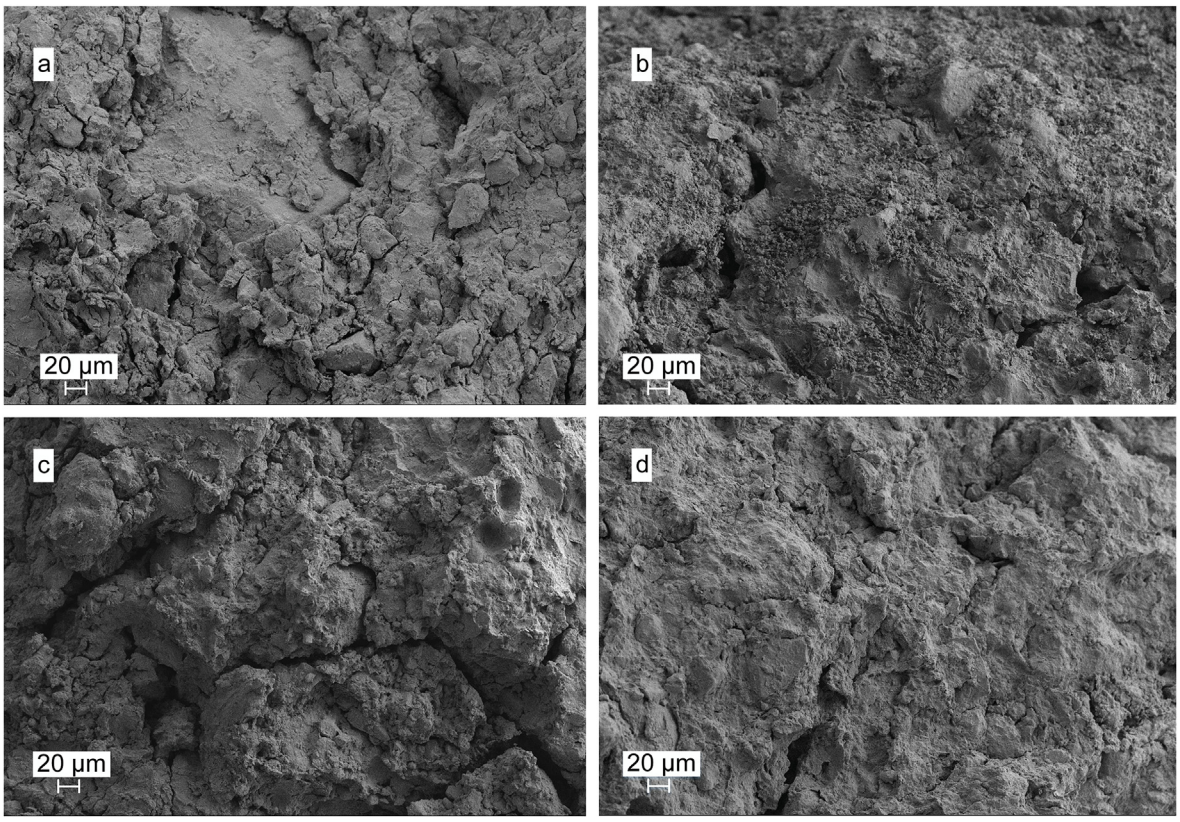

Fig. 7. FESEM images: (a) Saturated state, $N_{FT} = 10$, $c = 0$ mol/L; (b) Saturated state, $N_{FT} = 10$, $c = 3$ mol/L; (c) Air-dried state, $N_{FT} = 10$, $c = 0$ mol/L; and (d) Air-dried state, $N_{FT} = 10$, $c = 3$ mol/L.

saline intrusion that restrains the swelling of the soil matrix. However, the PSD curve in the macropore range changes significantly after the saline intrusion and becomes similar to that of as-compacted specimens (Figs. 5d and 8d). The dimension of the FT-induced cracks is not reduced (Figs. 2b and 7b), which means that the clay's healing (i.e. closure of cracks) is impaired during the saline intrusion.

Upon drying to the shrinkage limit, micropores shrink remarkably for specimens in both distilled water and 3 mol/L NaCl solution since their PSD curves (Fig. 8c and d) become flat and the V_m decreases. This is similar to that of specimens without FT histories. However, for the specimen saturated in distilled water, its PSD curve develops a new peak at 30 μm and the V_M increases significantly. This is due to the opening and widening of the FT-induced cracks during desiccation (Fig. 7c) that is associated with the shrinkage of the soil matrix.

The PSD curve of the specimen saturated in 3 mol/L NaCl solution also develops a similar peak close to 40 μm. However, its V_M remains almost constant during desiccation. This is the result of two reasons: (i) saline intrusion reduces the shrinkage of the soil matrix and (ii) the precipitated NaCl solid in macropores reduces the V_M. Comparing PSD curves in Figs. 5d and 8c and d, it can be seen that unlike the macropore space induced by the saline intrusion that shrinks significantly upon desiccation, the macropore space developed during FT cycles (i.e. FT-induced cracks) is less sensitive to desiccation.

3.2. Swelling behaviors

Fig. 9 shows examples of the development of swelling strain ε (the ratio of the volume of swelling to that of as-compacted specimens) versus time t for specimens with different N_{FT} values and saturated in distilled water, and as-compacted specimens ($N_{FT} = 0$) saturated in NaCl solution with different concentrations. The ε-t curves can be divided into initial swelling, primary swelling and secondary swelling phases (Rao et al., 2006; Zou et al., 2020a). Letters A and B in Fig. 9a were used to identify the boundaries of the three phases that are determined based on the graphical approach introduced by Zou et al. (2020a).

The swelling strain reduces significantly after just one FT cycle and the soil's volume is almost constant during saturation after 10 FT cycles. The ε-t curve becomes linear after FT cycles with less determinate boundaries between the three stages (Fig. 9a). Such behavior upon FT action is related to two reasons: (i) FT-induced cracks partly accommodate the swelling strain of the soil matrix from inside of the soil, which reduces the global swelling strain and results in the closure of the FT-induced cracks, and (ii) FT action facilitates further hydration of the surface of soil particles through water flow induced by the phase transition of water. A higher level of hydration results in less swelling (Day, 1994; Delage et al., 2006).

Similar to the effects of FT cycles, saline intrusion reduces the swelling of the as-compacted specimens (Fig. 9b). Such global volumetric behavior is consistent with the volumetric responses of the microstructure upon saline intrusion and is associated with the suppression of the electric double layer. Besides, the slope of the ε-t curves reduces and the initial and primary swelling stages are prolonged in salt solutions. This is owing to the osmotic pressure gradient between the inside and outside of the specimens that reduces the velocity of flow and thus the speed of swelling.

Fig. 10 shows the effects of saline intrusion and FT cycles on the final swelling strain (ε_f) of specimens. The ε_f reduces with increasing N_{FT} and c, and the ε_f-N_{FT} and ε_f-c relationships are nonlinear. The most significant reduction in the ε_f takes place during the first FT cycle and the initial increase in c. For the as-

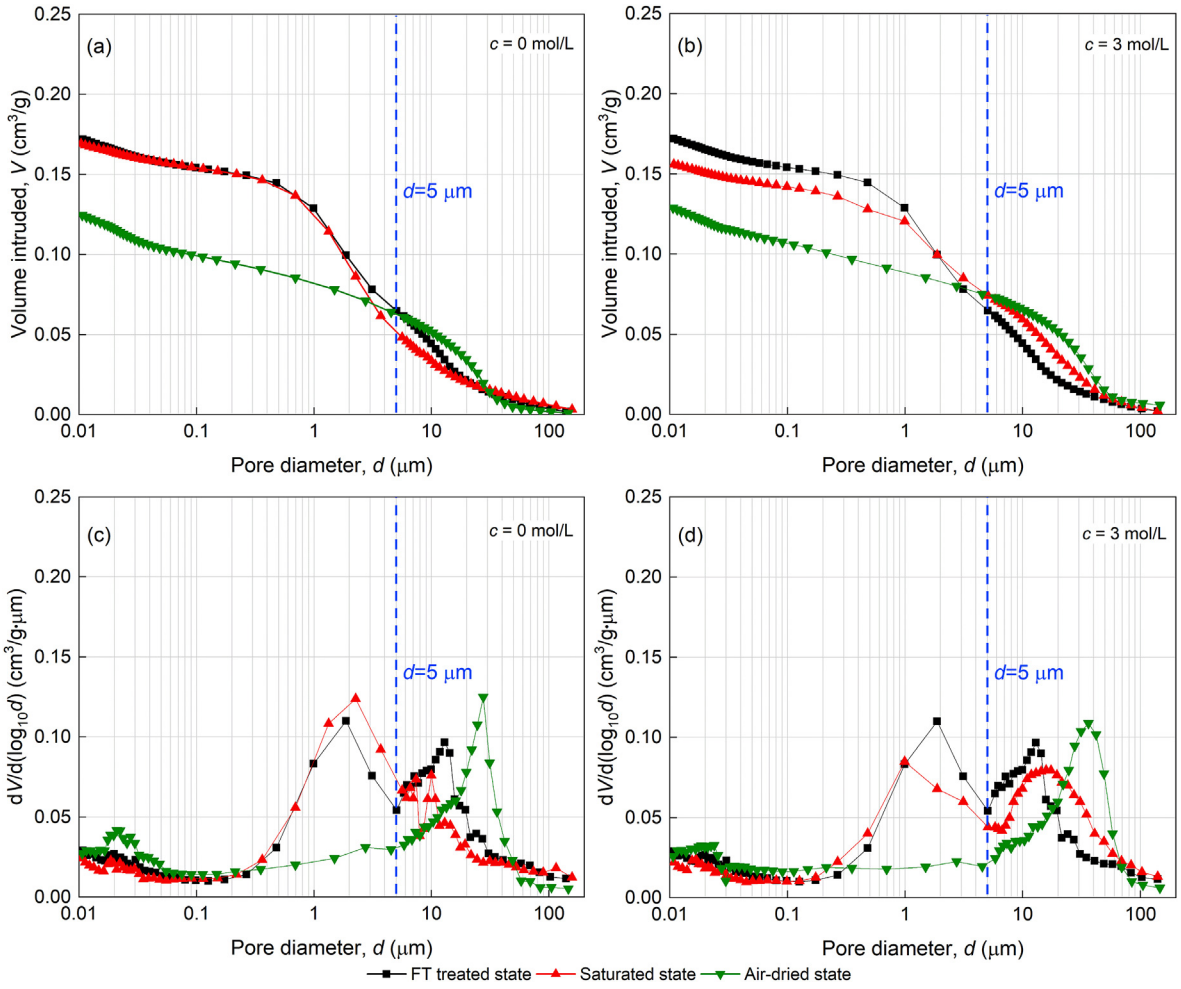

Fig. 8. MIP results of specimens with FT cycles: (a) CI curves at $c = 0$ mol/L, (b) CI curves at $c = 3$ mol/L, (c) PSD curves at $c = 0$ mol/L, (d) PSD curves at $c = 3$ mol/L.

compacted specimen, the ε_f reduces from 7.02% to 0.22% after 10 FT cycles, constituting a reduction of 97%, to 1.28% when inundated in 3 mol/L NaCl solution, constituting a reduction of 82%, and to 0.13% when subjected to10 FT cycles and then inundated in 3 mol/L NaCl solution, constituting a reduction of 98%. It can be seen that FT action is more effective in reducing the swelling potential of the tested clay compared to saline intrusion.

Fig. 11 shows the mass of (i) water and salt and (ii) salt that infiltrates into the specimens during inundation. The mass of intruded salt generally increases with the salt concentration, which is as expected and FT cycles appear to have little impact. NaCl solution suppresses the swelling of the soil and reduces the amount of absorbed water. Thus, the relationship of the mass of intruded water and salt with c is the interplay between two factors: reduction in the mass of water and the increase in the mass of salt. For the specimen without FT histories, the former factor governs and the mass of intruded water and salt reduces monotonically with c. When FT effects have come into an equilibrium (i.e. $N_{FT} = 10$), the former factor governs at low c (i.e. from 0 mol/L to 0.1 mol/L) and the later factor governs with a further increase in c (i.e. from 0.1 mol/L to 3 mol/L), resulting in a non-monotonic relationship.

3.3. Shrinkage behaviors

The shrinkage behavior of the tested clay during desiccation is described as the volumetric strain ε_v (defined by Eq. (2)) versus gravimetric water content w relationships (referred to as the shrinkage curve).

$$\varepsilon_v = \frac{V_1 - V_0}{V_0} \tag{2}$$

where V_1 is the volume of the specimen during shrinkage; and V_0 is the volume at the as-compacted state, which is a constant for all specimens.

Fig. 12 summarizes the influences of N_{FT} and saline intrusion on the shrinkage curves of the tested clay. A typical shrinkage curve has four stages, i.e. structural, basic, residual and zero shrinkage stages (Cornelis et al., 2006). The shrinkage curves obtained in this study present distinct basic and residual shrinkage stages. In general, their basic shrinkage stage is between w = 10% and 25%, as shown in Fig. 12. The slope of the shrinkage curve at the basic shrinkage stage (i.e. $\Delta\varepsilon_v/\Delta w$) is used to indicate the shrinkage behavior in this study. Table 3 summarizes the ε_v at oven-dryness (denoted as ε_{v0}), the total shrinkage during desiccation (i.e. differences betweenε_v at the saturated condition and ε_{v0}, denoted at ε_{vtotal}), and the slope of the shrinkage curve at the basic shrinkage stage.

The ε_{v0}, ε_{vtotal} and the slope generally decrease with increasing N_{FT} regardless of the concentration c of the pore fluid. This means that FT cycles reduce the soil's volumetric sensitivity during desiccation (i.e. shrinkage potential). On the other hand, for as-compacted and FT-impacted specimens, the ε_{v0}, ε_{vtotal} and the

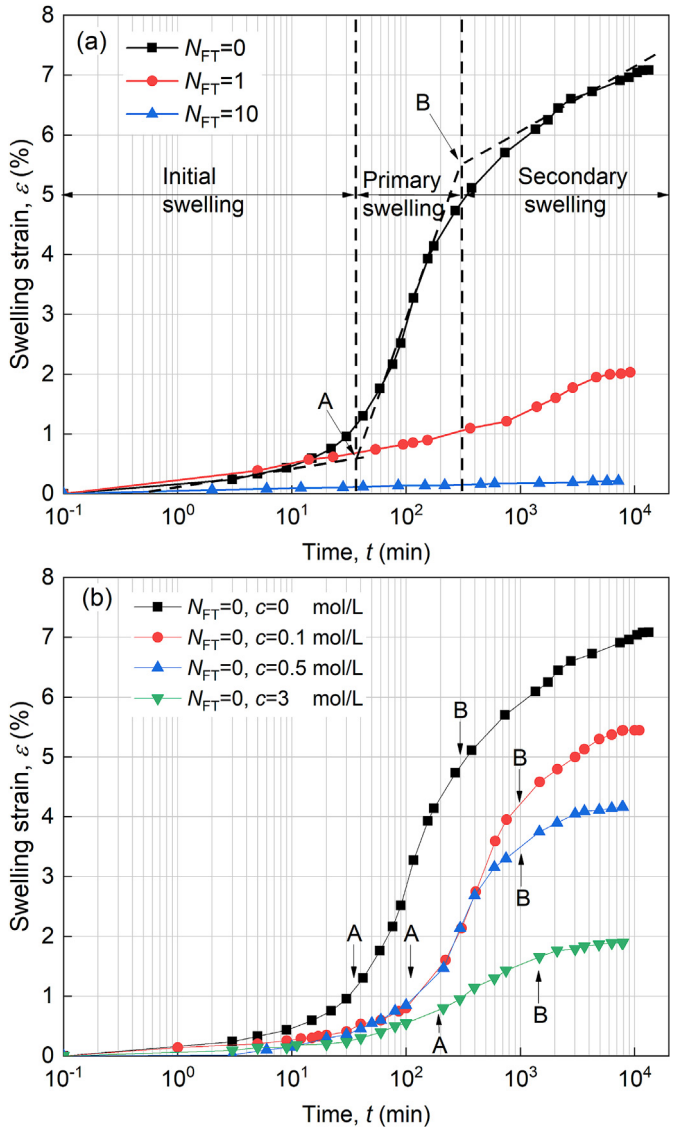

Fig. 9. Swelling strain-time relationships: (a) Specimens with different N_{FT} values and saturated in distilled water, and (b) As-compacted specimens saturated in NaCl solution with different c values.

slope generally first increase with c (from 0 mol/L to 0.1 mol/L or 0.5 mol/L) and then decrease with further increase in c (from 0.1 mol/L or 0.5 mol/L to 3 mol/L). These behaviors were also reported by Thyagaraj et al. (2017). The initial increase in the shrinkage potential is associated with the osmotic consolidation and osmotically-induced consolidation triggered by the saline intrusion. With increasing c, although such effects still exist, the increase in the volume of undissolved salt crystals results in an increase in the final volume of solid phase in the specimens and thus the decrease in the shrinkage potential.

Rijniersce (1983) first proposed a geometry factor, γ_s, to describe the relationship between the vertical and horizontal shrinkage, as written by

$$1-\frac{\Delta V}{V_{sat}}=\left(1-\frac{\Delta Z}{Z_{sat}}\right)^{\gamma_s} \tag{3}$$

where V_{sat} is the soil bulk volume at saturated condition; ΔV is the volume change upon shrinkage; Z_{sat} is the height of specimens at saturated condition; ΔZ is the change in the height of specimens upon shrinkage; $\gamma_s = 1$ means 1D vertical subsidence, and $\gamma_s = 3$ indicates three-dimensional (3D) isotropic shrinkage.

Fig. 13 summarizes the relationships between γ_s and w. Generally, γ_s increases from 1 to around 3 with decreasing w, meaning that the shrinkage is approximately 1D when specimens are saturated and the shrinkage gradually becomes isotropic during desiccation. Such behavior is consistent with similar experimental results reported by Rijniersce (1983) and is associated with the changes in the degree of orientation of clay particles.

Clay particles after compaction demonstrate a high degree of particle orientation with mainly face-to-face contacts. Clay particles are generally perpendicular to the direction of compaction, as shown in Fig. 14a. The saturation process does not significantly alter the degree of particle orientation. Upon desiccation, the shrinkage mainly takes place in the direction that is perpendicular to the orientation of clay particles. During the initial stage of desiccation, due to the high degree of particle orientation, the shrinkage mainly takes place in the vertical direction, constituting the 1D shrinkage. With further shrinkage, the orientation of clay particles gradually changes, which increases the amount of clay particles that face the lateral direction and face-to-point contacts (Fig. 14b). Due to this reason, the degree of particle orientation reduces and the lateral shrinkage develops, rendering the 1D vertical shrinkage to 3D shrinkage.

Specimens tend to demonstrate isotropic shrinkage at a higher w level after subjecting to FT cycles (i.e. γ_s increases after FT cycles). In other words, FT cycles facilitate the horizontal shrinkage at a higher w level. This is owing to the effects of FT cycles on the orientation of clay particles. It appears that FT cycles reduce the degree of particle orientation and facilitate the development of lateral shrinkage during the early stage of desiccation. The NaCl solution appears to exert the opposite effect. At the same w level, γ_s of saline intruded specimens decreases with increasing c. This means that the NaCl solution increases the degree of particle orientation and thus suppresses the lateral shrinkage during the early stage of desiccation.

3.4. Water retention behaviors

Fig. 15 presents the SWRCs obtained from the filter paper method in terms of total suction, s (referred to as s-SWRCs). The concentration of the pore fluid directly influences the osmotic suction that is a part of the total suction. Consequently, the s-SWRCs are sensitive to the changes in c of the NaCl solution, especially at the high concentration ($c = 3$ mol/L). At a certain w level, s increases with c, leading to a right-upward rotation of the s-SWRCs for specimens with different FT histories (Fig. 15a–c). With the increase in s, all s-SWRCs tend to converge to $w = 0$ and $s = 10^6$ kPa, which is consistent with the assumption of Fredlund and Xing (1994) that the maximum suction at the dry condition is 10^6 kPa.

FT cycles mainly reduce the water retention capacity of the soil in the low suction range (i.e. $s < 10^4$ kPa), which is reflected by a downshifting of the s-SWRCs. This is associated with the reduction in the pore space of micropores where the majority of capillary water is stored (Monroy et al., 2010; Alaoui et al., 2011). It is noted that macropores desaturate at very low suction (typically at several kilopascals) due to their large pore radius, especially after FT cycles. In the high suction range (i.e. $s > 10^4$ kPa), only adsorbed water is retained in the soil which is not sensitive to the FT-induced structural changes. Thus, the s-SWRCs remain unchanged after FT cycles (Fig. 15d–f).

Fig. 16 presents the SWRCs obtained from the filter paper method in terms of matric suction, s_m (referred to as s_m-SWRCs).

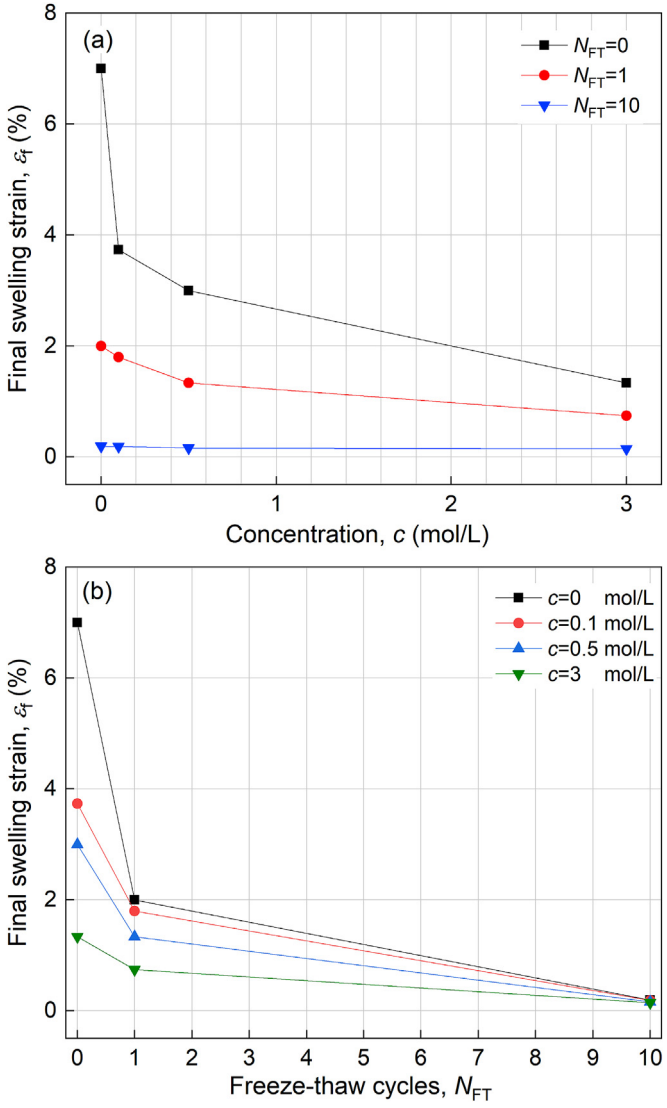

Fig. 10. Relationships of ε_f with (a) c and (b) N_{FT}.

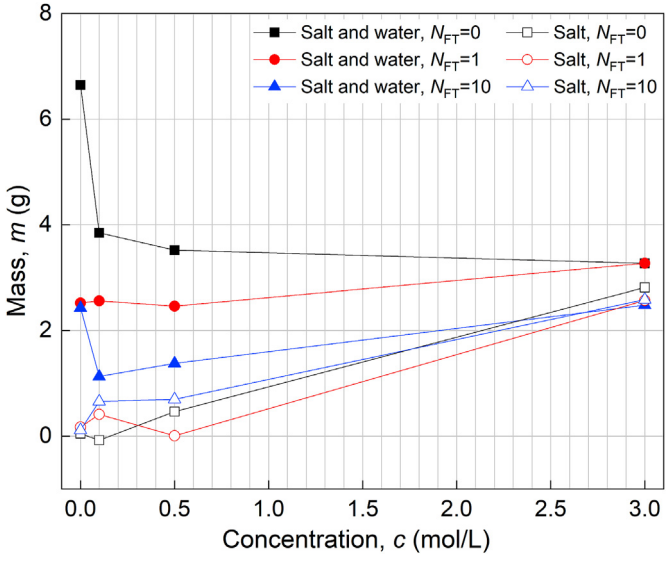

Fig. 11. Mass of intruded water and salt during saturation process.

Measurements were fitted using the model proposed by Fredlund and Xing (1994) as

$$w = w_{sat}\left[1-\frac{\ln(1+s/s_{res})}{\ln\left(1+10^6/s_{res}\right)}\right]\left\{\ln\left[2.718+(s/a)^n\right]\right\}^{-m} \quad (4)$$

where s_{res} is the residual suction and takes the value of 10^5 kPa; w_{sat} is the moisture content at saturated condition; and a, n and m are the model parameters. Model parameters are summarized in

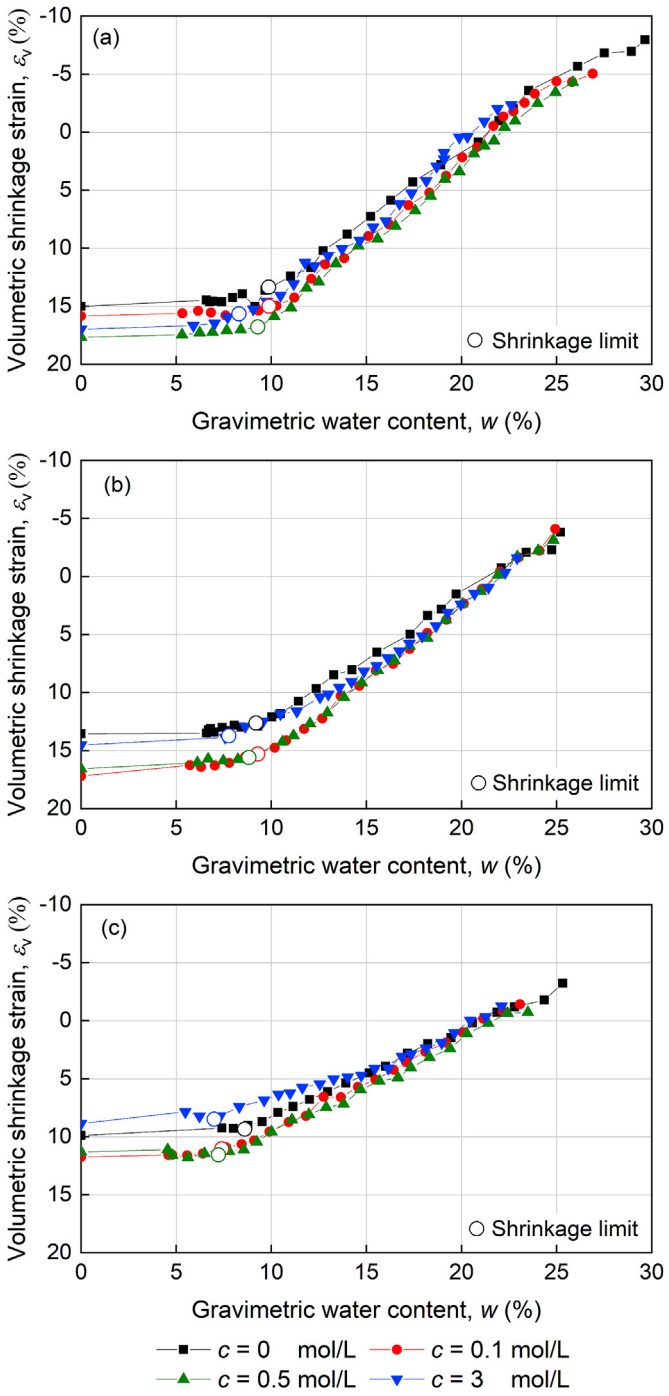

Fig. 12. Shrinkage curves of specimens with (a) $N_{FT} = 0$, (b) $N_{FT} = 1$, and (c) $N_{FT} = 10$.

Table 3
Characteristics of the shrinkage curves at different concentrations.

N_{FT}	Characteristic	Value			
		c = 0 mol/L	c = 0.1 mol/L	c = 0.5 mol/L	c = 3 mol/L
0	Slope of shrinkage curve	120.78	133.7	132.4	136.36
	Final volumetric strain, ε_{v0} (%)	15.01	15.85	17.68	16.99
	Total shrinkage, ε_{vtotal} (%)	22.83	20.95	22.02	19.35
1	Slope of shrinkage curve	106.73	128.39	128.35	110.58
	Final volumetric strain, ε_{v0} (%)	13.55	17.2	16.57	14.52
	Total shrinkage, ε_{vtotal} (%)	17.35	21.28	19.59	16.48
10	Slope of shrinkage curve	74.9	84.77	82.03	57.61
	Final volumetric strain, ε_{v0} (%)	9.89	11.74	11.31	8.84
	Total shrinkage, ε_{vtotal} (%)	13.13	13.19	12.1	10.09

Table 4, along with the coefficient of determination R^2 achieved for each SWRC.

The concentration of the pore fluid shows much less influence on the s_m-SWRCs compared to the s-SWRCs. Changes in the s_m-SWRCs are negligible when c increases from 0 mol/L to 0.1 mol/L (Fig. 16a–c), although the swelling and shrinkage behaviors change substantially. The slope of the s_m-SWRCs slightly reduces when c further increases from 0.1 mol/L to 3 mol/L. This is possibly due to the changes in the soil's macropores and micropores upon saline intrusion. Based on these observations, it can be concluded that the salinity mainly influences the clay's volumetric and water-retention behavior through adsorption effects instead of capillary effects.

Similar to the responses of s-SWRCs, the s_m-SWRCs shift downward in the low suction range upon FT cycles, indicating a reduction in the water retention capacity (Fig. 16d–f). The s_m-SWRCs in the high suction range are less affected. It is noted that the variation in the s_m-SWRCs upon FT cycles becomes less significant as c increases.

Table 5 summarizes the measured and calculated osmotic suctions. The osmotic suction increases with salt concentration and FT cycles appear to have insignificant influence. For specimens inundated with distilled water (c = 0 mol/L), the measured osmotic suction is about 600 kPa. Such osmotic suction is associated with the intrinsically dissolved salt existing in the native clay. For specimens inundated with 0.1 mol/L and 3 mol/L salt solution, the measured osmotic suction value is close to the calculated one plus the measured osmotic suction at c = 0 mol/L. This implies that the concentration of the pore fluid inside the soil equals the concentration of NaCl solution used for soaking the specimens, and the osmotic suction measured from the filter paper method is reliable.

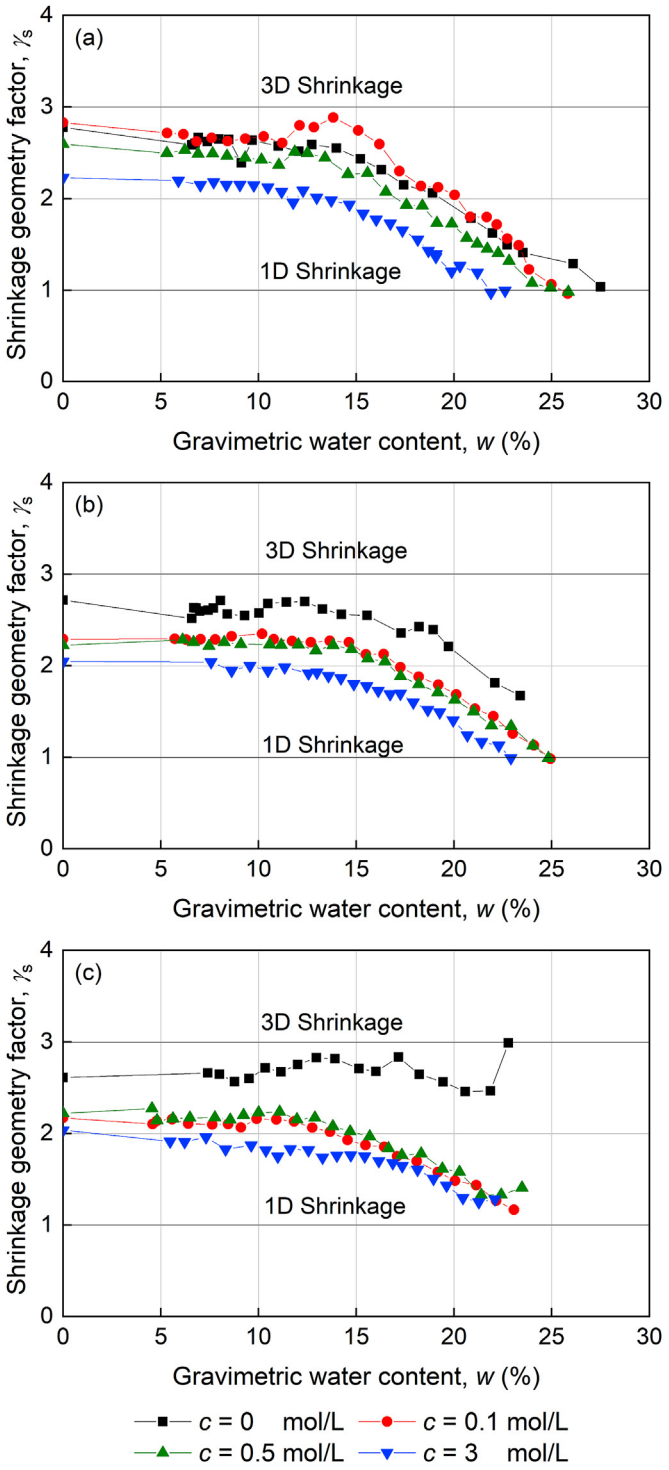

Fig. 13. γ_s-w relationships at (a) N_{FT} = 0, (b) N_{FT} = 1, and (c) N_{FT} = 10.

4. Conclusions

Effects of FT cycles and saline intrusion on the structural, volumetric and water retention behaviors of a compacted clay during swelling and shrinkage processes were investigated in this study. The following conclusions are drawn from the experimental results:

(1) Both FT cycles and salinization reduce the clay's micropore space and increase its macropore space. FT cycles influence the pore structure through the migration of water between the micropores and macropores and the development of ice crystals while salinization influences the pore structure by altering the thickness of the electric double layer between soil particles. Salinization reduces the swelling of the soil matrix and thus suppresses the healing of the FT-induced cracks during soaking. The FT-induced macropore space develops during desiccation due to the opening and widening of the FT-induced cracks, while salinization-induced macropore space shrinks significantly during desiccation. Micropore space significantly shrinks during desiccation regardless of the FT history and saline intrusion.

(2) The swelling potential of specimens reduces significantly after FT actions because FT-induced cracks accommodate the swelling of the soil matrix and FT cycles facilitate further

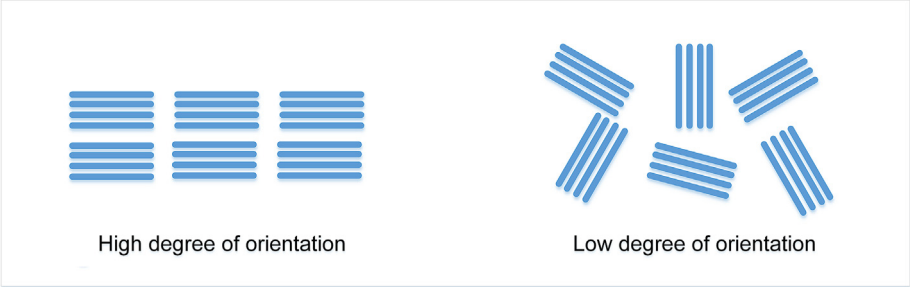

Fig. 14. Orientation of clay particles.

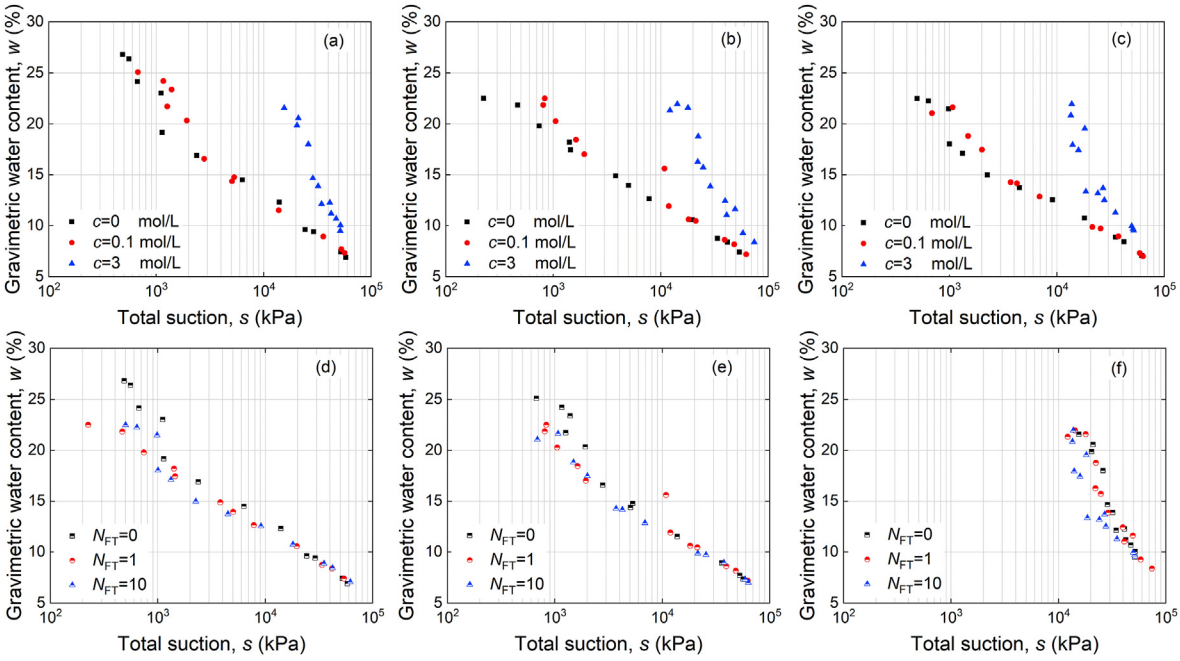

Fig. 15. s-SWRCs at (a) $N_{FT} = 0$, (b) $N_{FT} = 1$, (c) $N_{FT} = 10$, (d) $c = 0$ mol/L, (e) $c = 0.1$ mol/L, and (f) $c = 3$ mol/L.

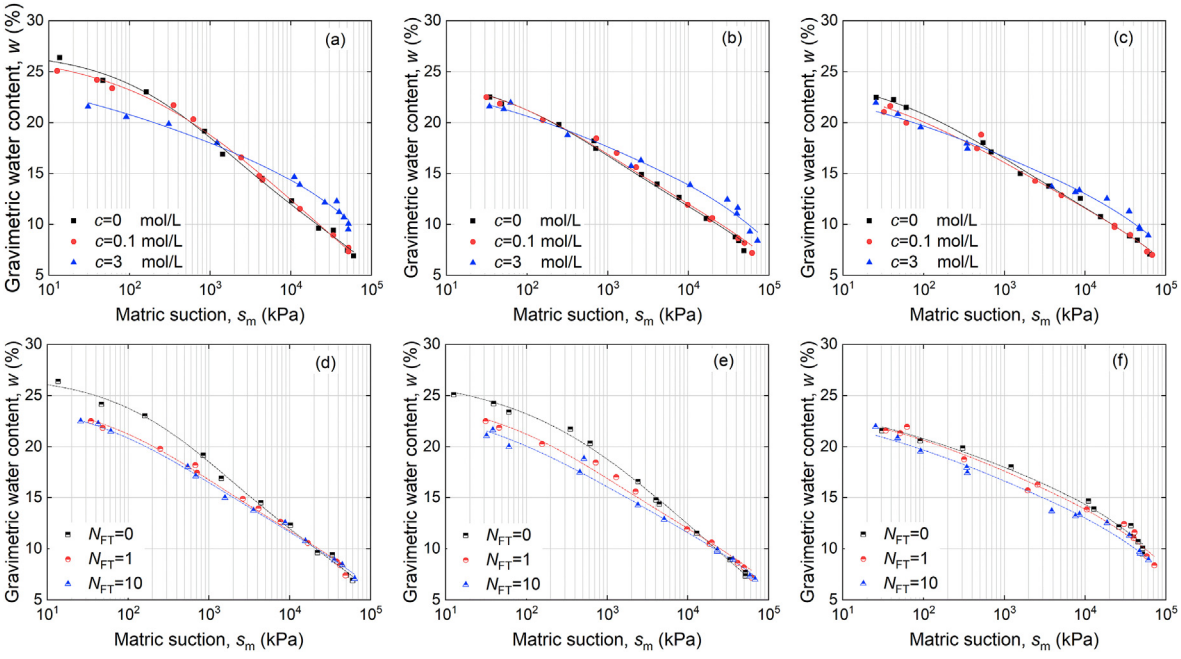

Fig. 16. s_m-SWRCs at (a) $N_{FT} = 0$, (b) $N_{FT} = 1$, (c) $N_{FT} = 10$, (d) $c = 0$ mol/L, (e) $c = 0.1$ mol/L, and (f) $c = 3$ mol/L.

Table 4
Model parameters of the Fredlund and Xing (1994)'s SWRC model.

N_{FT}	Parameter	Value		
		c = 0 mol/L	c = 0.1 mol/L	c = 3 mol/L
0	a	443	2090	3000
	m	0.97	1.69	1.78
	n	0.6	0.44	0.23
	w_{sat}	0.29	0.27	0.26
	R^2	1	1	0.99
1	a	210	210	210
	m	0.82	0.81	0.86
	n	0.54	0.53	0.35
	w_{sat}	0.25	0.25	0.25
	R^2	0.99	0.99	0.98
10	a	210	210	210
	m	0.89	1.02	1.05
	n	0.5	0.41	0.31
	w_{sat}	0.25	0.23	0.23
	R^2	1	0.99	0.98

Table 5
Measured and calculated osmotic suctions.

c (mol/L)	Osmotic suction (kPa)			
	Calculated (Eq. (1))	Measured		
		N_{FT}=0	N_{FT}=1	N_{FT}=10
0		549	548	666
0.1	496	1039	819	958
3	14,873	18,847	14,743	15,088

hydration. Salinization also reduces the swelling of specimens and prolongs their primary and secondary swelling stages.

(3) The clay's shrinkage potential reduces remarkably after FT cycles because of the FT cracks. The shrinkage potential initially increases with the concentration of the pore-fluid due to the osmotic consolidation and osmotically-induced consolidation. The shrinkage potential tends to decrease with the further increase in the concentration because of the precipitated salt crystals. Besides, FT cycles facilitate the horizontal shrinkage at a higher water level, while the NaCl solution appears to exert opposite effects. This may be attributed to the degree of particle orientation which decreases with increasing N_{FT} but increases with increasing concentration of the pore-fluid.

(4) Total suction increases with the concentration of saline solution due to the contribution of osmotic suction regardless of FT cycles. However, the concentration of pore fluid shows much less influence on matric suction compared to the total suction. FT cycles reduce the water retention capacity of the clay at low suction levels but have little impact on the water retention capacity at high suction levels.

Declaration of competing interest

The authors declare that they have no known competing financial interests or personal relationships that could have appeared to influence the work reported in this paper.

Acknowledgments

The research was supported by the National Natural Science Foundation of China (Grant Nos. 51779191 and 51809199), which is highly appreciated.

References

ASTM D5298-10, 2010. Standard Test Method for Measurement of Soil Potential (Suction) Using Filter Paper. ASTM International, West Conshohocken, PA, USA.
ASTM D4546-14, 2019. Standard Test Methods for One-Dimensional Swell or Collapse of Soils. ASTM International, West Conshohocken, PA, USA.
Alaoui, A., Lipiec, J., Gerke, H.H., 2011. A review of the changes in the soil pore system due to soil deformation: a hydrodynamic perspective. Soil Tillage Res. 115–116, 1–15.
Barbour, S.L., Fredlund, D.G., 1989. Mechanisms of osmotic flow and volume change in clay soils. Can. Geotech. J. 26 (4), 551–562.
Basma, A.A., Al-Homoud, A.S., Husein Malkawi, A.I., Al-Bashabsheh, M.A., 1996. Swelling-shrinkage behavior of natural expansive clays. Appl. Clay Sci. 11 (2), 211–227.
Birle, E., Heyer, D., Vogt, N., 2008. Influence of the initial water content and dry density on the soil–water retention curve and the shrinkage behavior of a compacted clay. Acta Geotech 3 (3), 191–200.
Boivin, P., Garnier, P., Tessier, D., 2004. Relationship between clay content, clay type, and shrinkage properties of soil samples. Soil Sci. Soc. Am. J. 68 (4), 1145.
Bolt, G.H., 1955. Analysis of the validity of the Gouy-Chapman theory of the electric double layer. J. Colloid Sci. 10 (2), 206–218.
Burton, G.J., Pineda, J.A., Sheng, D.C., Airey, D., 2015. Microstructural changes of an undisturbed, reconstituted and compacted high plasticity clay subjected to wetting and drying. Eng. Geol. 193, 363–373.
Castellanos, E., Villar, M.V., Romero, E., Lloret, A., Gens, A., 2008. Chemical impact on the hydro-mechanical behaviour of high-density FEBEX bentonite. Phys. Chem. Earth, Parts A/B/C 33, S516–S526.
Chamberlain, E.J., 1973. A model for predicting the influence of closed system freeze-thaw on the strength of thawed clays. In: Proceedings of the Symposium on Frost Action on Roads. Paris.
Chamberlain, E.J., Gow, A.J., 1979. Effect of freezing and thawing on the permeability and structure of soils. Eng. Geol. 13 (1–4), 73–92.
Chertkov, V.Y., 2007. The reference shrinkage curve at higher than critical soil clay content. Soil Sci. Soc. Am. J. 71 (3), 641.
Cui, Y., Tang, A.M., 2013. On the chemo-thermo-hydro-mechanical behaviour of geological and engineered barriers. J. Rock Mech. Geotech. Eng 5 (3), 169–178.
Cornelis, W.M., Corluy, J., Medina, H., Díaz, J., Hartmann, R., Van Meirvenne, M., Ruiz, M.E., 2006. Measuring and modelling the soil shrinkage characteristic curve. Geoderma 137 (1–2), 179–191.
Dalla Santa, G., Cola, S., Secco, M., Tateo, F., Sassi, R., Galgaro, A., 2019. Multiscale analysis of freeze–thaw effects induced by ground heat exchangers on permeability of silty clays. Geotechnique 69 (2), 95–105.
Daniel, D.E., Wu, Y.K., 1993. Compacted clay liners and covers for arid sites. J. Geotech. Eng 119 (2), 223–237.
Day, R.W., 1994. Swell-shrink behavior of compacted clay. J. Geotech. Eng 120 (3), 618–623.
Delage, P., Marcial, D., Cui, Y.J., Ruiz, X., 2006. Ageing effects in a compacted bentonite: A microstructure approach. Géotechnique 56 (5), 291–304.
Deneele, D., Cuisinier, O., Hallaire, V., Masrouri, F., 2010. Microstructural evolution and physico-chemical behavior of compacted clayey soil submitted to an alkaline plume. J. Rock Mech. Geotech. Eng 2 (2), 169–177.
Di Maio, C., 1996. Exposure of bentonite to salt solution: osmotic and mechanical effects. Geotechnique 46 (4), 695–707.
Ding, L., Han, Z., Zou, W., Wang, X., 2020. Characterizing hydro-mechanical behaviours of compacted subgrade soils considering effects of freeze-thaw cycles. Transp. Geotech 24, 100392.
Fredlund, D.G., Xing, A., 1994. Equations for the soil-water characteristic curve. Can. Geotech. J. 31 (4), 521–532.
GB/T 50123-2019, 2019. Standards for Geotechnical Testing Method. Ministry of Water Resources, Beijing, China.
Gens, A., 2010. Soil-environment interactions in geotechnical engineering. Geotechnique 60 (1), 3–74.
Han, Z., Vanapalli, S.K., 2017. Normalizing variation of stiffness and shear strength of compacted fine-grained soils with moisture content. J. Geotech. Geoenviron. Eng. 143 (9), 04017058.
He, Y., Ye, W.M., Chen, Y.G., Chen, B., Ye, B., Cui, Y., 2016. Influence of pore fluid concentration on water retention properties of compacted GMZ01 bentonite. Appl. Clay Sci. 129, 131–141.
Jobmann, M., Bebiolka, A., Burlaka, V., et al., 2017. Safety assessment methodology for a German high-level waste repository in clay formations. J. Rock Mech. Geotech. Eng 9 (5), 856–876.
Julina, M., Thyagaraj, T., 2020. Combined effects of wet-dry cycles and interacting fluid on desiccation cracks and hydraulic conductivity of compacted clay. Eng. Geol. 267, 105505.
Konrad, J.M., 1989. Physical processes during freeze-thaw cycles in clayey silts. Cold Reg. Sci. Technol. 16 (3), 291–303.
Leong, E.C., Wijaya, M., 2015. Universal soil shrinkage curve equation. Geoderma 237–238, 78–87.
Liu, J., Chang, D., Yu, Q., 2016. Influence of freeze-thaw cycles on mechanical properties of a silty sand. Eng. Geol. 210, 23–32.
Lu, N., 2016. Generalized soil water retention equation for adsorption and capillarity. J. Geotech. Geoenviron. Eng. 142 (10), 4016051.
Lu, N., Khorshidi, M., 2015. Mechanisms for soil-water retention and hysteresis at high suction range. J. Geotech. Geoenviron. Eng. 141 (8), 4015032.

Lu, N., Dong, Y., 2017. Correlation between soil-shrinkage curve and water-retention characteristics. J. Geotech. Geoenviron. Eng. 143 (9), 4017054.
Lu, Y., Liu, S., Alonso, E., Wang, L., Xu, L., Li, Z., 2019. Volume changes and mechanical degradation of a compacted expansive soil under freeze-thaw cycles. Cold Reg. Sci. Technol. 157, 206–214.
Lyu, C., Sun, Q., Zhang, W., 2020. Effects of NaCl concentration on thermal conductivity of clay with cooling. Bull. Eng. Geol. Environ. 79, 1449–1459.
Mishra, P.N., Scheuermann, A., Bore, T., Li, L., 2019. Salinity effects on soil shrinkage characteristic curves of fine-grained geomaterials. J. Rock Mech. Geotech. Eng 11 (1), 181–191.
Mitchell, J.K., Hooper, D.R., Campanella, R.G., 1965. Permeability of compacted clay. J. Soil Mech. Found Div. 91 (4), 41–65.
Mokni, N., Romero, E., Olivella, S., 2014. Chemo-hydro-mechanical behaviour of compacted Boom Clay: joint effects of osmotic and matric suctions. Geotechnique 64 (9), 681–693.
Molinero-Guerra, A., Delage, P., Cui, Y., et al., 2020. Water-retention properties and microstructure changes of a bentonite pellet upon wetting/drying; application to radioactive waste disposal. Geotechnique 70 (3), 199–209.
Monroy, R., Zdravkovic, L., Ridley, A., 2010. Evolution of microstructure in compacted London Clay during wetting and loading. Geotechnique 60 (2), 105–119.
Musso, G., Romero, E., Vecchia, G.D., 2013. Double-structure effects on the chemo-hydro-mechanical behaviour of a compacted active clay. Geotechnique 63 (3), 206–220.
Musso, G., Romero Morales, E., Gens, A., Castellanos, E., 2003. The role of structure in the chemically induced deformations of FEBEX bentonite. Appl. Clay Sci. 23 (1–4), 229–237.
Palomino, A.M., Santamarina, J.C., 2005. Fabric map for kaolinite: effects of pH and ionic concentra-tion on behavior. Clay Miner. 53 (3), 211–223.
Qi, J., Vermeer, P.A., Cheng, G., 2006. A review of the influence of freeze-thaw cycles on soil geotechnical properties. Permafr. Periglac. Process. 17 (3), 245–252.
Rao, S.M., Shivananda, P., 2005. Role of osmotic suction in swelling of salt-amended clays. Can. Geotech. J. 42 (1), 307–315.
Rao, S.M., Thyagaraj, T., 2007. Swell–compression behaviour of compacted clays under chemical gradients. Can. Geotech. J. 44 (5), 520–532.
Rao, S.M., Thyagaraj, T., 2010. Influence of osmotic suction on the soil-water characteristic curves of compacted expansive clay. J. Geotech. Geoenviron. Eng. 136 (12), 1695–1702.
Rao, S.M., Thyagaraj, T., Thomas, H.R., 2006. Swelling of compacted clay under osmotic gradients. Geotechnique 56 (10), 707–713.
Ren, J., Vanapalli, S.K., Han, Z., 2017. Soil freezing process and different expressions for the soil-freezing characteristic curve. Sci. Cold Arid Reg 9 (3), 221–228.
Rijniersce, K., 1983. A Simulation Model for Physical Soil Ripening in the Ijsselmeerpolders. Rijksdienst voor de IJsselmeerpolders, Lelystad, the Netherlands.
Romero, E., Gens, A., Lloret, A., 1999. Water permeability, water retention and microstructure of unsaturated compacted Boom clay. Eng. Geol. 54 (1), 117–127.
Romero, E., Della vecchia, G., Jommi, C., 2011. An insight into the water retention properties of compacted clayey soils. Geotechnique 61 (4), 313–328.
Thyagaraj, T., Rao, S.M., 2010. Influence of osmotic suction on the soil-water characteristic curves of compacted expansive clay. J. Geotech. Geoenviron. Eng. 136 (12), 1695–1702.
Thyagaraj, T., Rao, S.M., 2013. Osmotic swelling and osmotic consolidation behaviour of compacted expansive clay. Geotech. Geol. Eng. 31 (2), 435–445.
Thyagaraj, T., Thomas, S.R., Das, A.P., 2017. Physico-chemical effects on shrinkage behavior of compacted expansive clay. Int. J. GeoMech. 17 (2), 6016013.
Toker, N.K., Germaine, J.T., Sjoblom, K.J., Culligan, P.J., 2004. A new technique for rapid measurement of continuous soil moisture characteristic curves. Geotechnique 54 (3), 179–186.
Zhang, Y., Ye, W., Chen, Y., Chen, B., 2017. Impact of NaCl on drying shrinkage behavior of low-plasticity soil in earthen heritages. Can. Geotech. J. 54 (12), 1762–1774.
Zou, W., Han, Z., Ye, J., 2020a. Influence of external stress and initial density on the volumetric behavior of an expansive clay during wetting. Environ. Earth Sci. 79 (10), 211.
Zou, W., Ding, L., Han, Z., Wang, X., 2020b. Effects of freeze-thaw cycles on the moisture sensitivity of a compacted clay. Eng. Geol. 278, 105832.
Zou, W., Ye, J., Han, Z., Vanapalli, S.K., Tu, H., 2018a. Effect of montmorillonite content and sodium chloride solution on the residual swelling pressure of an expansive clay. Environ. Earth Sci. 77 (19).
Zou, W., Han, Z., Vanapalli, S.K., Zhang, J., Zhao, G., 2018b. Predicting volumetric behavior of compacted clays during compression. Appl. Clay Sci. 156, 116–125.

Weilie Zou obtained his BSc degree in Hydraulic Structure and MSc degree in Geotechnical Engineering from Wuhan University of Hydraulic and Electric Engineering, China, in 1992 and 1997, respectively, and his PhD in Geotechnical Engineering in 2004 from Wuhan University, China. He worked as engineer in Shenzhen Municipal Co. Ltd. during 1999–2000, and was employed by Wuhan University from 2000 till present. He was appointed full professor at Wuhan University in 2009, and was a Vice Dean of School of Civil Engineering, Wuhan University during 2016–2020. His research interests cover unsaturated soil mechanics, application principal of geosynthetics, laboratory testing, constitutive modeling, transportation geotechnics, lime/cement stabilized soils, etc.